ACS APPLIED
OPTICAL MATERIALS

Editors' Choice

pubs.acs.org/acsaom Article

Functionalization of Monolayer MoS_2 with Layered Multimolecular Architectures

Ashley Arcidiacono,* Cooper R. Johnston, Clare L. Keenan, Nasim Mirzajani, Anoushka Ghosh, Alexander S. Filatov, and Sarah B. King*

Cite This: *ACS Appl. Opt. Mater.* 2024, 2, 2011−2018 **Read Online**

ACCESS | Metrics & More | Article Recommendations | Supporting Information

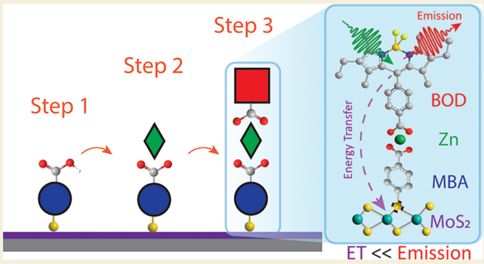

ABSTRACT: Two dimensional van der Waals materials have attracted attention due to their unique properties that arise in the monolayer versus bulk limits. Monolayer MoS_2 has been at the forefront of 2D materials due to its broad applicability in catalysis, photovoltaics, and spintronics. To realize the capabilities of MoS_2 enabled technology, it is necessary to engineer interfaces where charge carriers can be funneled toward or away from the surface. Molecular systems are a versatile strategy to enable this. Ion-linked molecular architectures have been used previously to circumvent difficult and taxing synthetic methods. Here, we demonstrate the growth of metal ion-linked bilayers (ILBs) on monolayer MoS_2 consisting of a first layer spacer (4-mercaptobenzoic acid, MBA) with a Zn(II) ion linked to a fluorophore (BODIPY). Using a combination of Atomic Force Microscopy and Raman spectroscopy, we resolved intrinsic S-vacancies in the MoS_2 lattice via S−H bond breaking of MBA. X-ray Photoelectron Spectroscopy confirmed that Zn(II) acetate can coordinate to carboxylate groups on MBA. With photoluminescence microscopy, we determined that BODIPY emission is observable only in the presence of a metal ion, confirming the growth of a multimolecular ion-linked supramolecular assembly on MoS_2.

KEYWORDS: *ion linked bilayers, monolayer MoS_2, self-assembly, thin films, TMD optical functionalization*

INTRODUCTION

Transition metal dichalcogenides (TMDs) have garnered significant interest due to their wide applicability in photocatalysis, p/n heterojunctions, and photonics.[1−4] Excitons in TMDs are highly sensitive to their local dielectric environment because the excitonic fields are not confined inside the 2D layer.[5,6] This environmental sensitivity provides extensive opportunities for modulation of the optoelectronic properties of TMDs through doping, patterning, and strain.[7−12]

While TMDs can be grown in small scale batches with low defect density[13−15] using Chemical Vapor Deposition (CVD), at production scale sulfur vacancies are ubiquitous. Although these vacancies can be detrimental and impede charge transport in devices by acting as charge trap sites,[16,17] they also provide a platform for functionalizing TMD surfaces with thiolated molecules.[18,19] Functionalization techniques include thermal evaporation, drop casting, covalent functionalization via click reactions, and edge-site defect healing.[20−27] Makarova et al.[28] demonstrated that thiol groups could be used to selectively chemisorb organic molecules to S-vacancies on the basal plane of MoS_2. Earlier work from Moehl et al.[29] also suggested such a binding motif, but the atomic resolution afforded by STM allowed Makarova et al.[28] to atomistically control the generation of S-vacancies and thiol adsorption. Covalent adsorption of thiolated molecules to S-vacancies in MoS_2 has been used in molecular p/n doping,[30] catalysis,[31] and protein targeted biosensors.[32] However, as we seek to engineer increasingly sophisticated electrocatalytic systems, biofunctionalize surfaces for bioresponsive labeling, and develop energy and charge carrier cascades, it is necessary to extend our functionalization strategies to allow for highly customized and robust designer surfaces.

Ion-linked bilayers (ILBs) have emerged as a simple, modular strategy for the adsorption of molecules on a wide range of materials, from planar metal and metal oxide surfaces to nanoparticle films.[33] ILBs are grown through a simple, stepwise soaking approach, where the first molecular layer is added to a surface via adsorption with appropriate surface binding groups prior to the sequential addition of further layers.[34,35] The first layer molecules contain a geometrically opposed metal ion binding group (typically −COOH or $-PO_3H_2$). The linking ion is then added by soaking the first layer in a metal acetate salt solution. Finally, the last layer is attached to the linked metal ion via carboxylate coordination. This stepwise loading procedure can be done repeatedly, with

Received: July 26, 2024
Revised: August 30, 2024
Accepted: September 2, 2024
Published: September 16, 2024

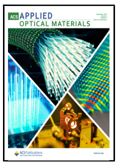

https://doi.org/10.1021/acsaom.4c00327
ACS Appl. Opt. Mater. 2024, 2, 2011−2018

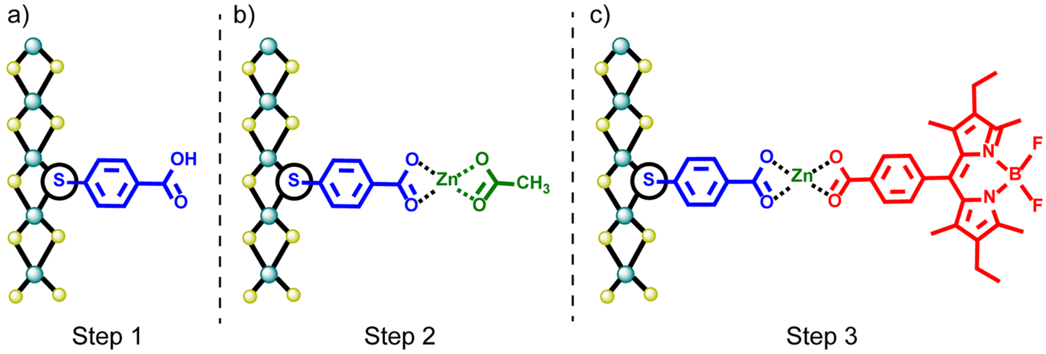

Figure 1. Three-step growth of ILBs on MoS_2 consisting of (from left to right) soaking in (a) MBA (blue), then (b) $Zn(OAc)_2$ (green), and last (c) BODIPY(red).

previous studies on planar metal oxides suggesting robust growth up to 65 layers.[36] ILBs have shown promise in diverse applications ranging from p/n heterojunctions to electron donor/acceptor cascades to dye-sensitized solar cells.[37−42]

In this paper, we demonstrate the growth of metal ion-linked molecular bilayers on MoS_2 surfaces, Figure 1. These assemblies are built by first adsorbing a thiolated organic molecule (MBA, blue in Figure 1) to S-vacancies that are generated during the CVD growth of MoS_2. We then attach a Zn(II) linking ion (green in Figure 1), which allows for the addition of a fluorescent probe (BODIPY, red in Figure 1). We envision this work will be broadly applicable to any S-containing TMD material system, opening up the field of flexible and robust supramolecular assembly on sulfur-containing TMD materials.

■ EXPERIMENTAL METHODS

Materials

4-mercaptobenzoic acid (MBA), Zinc acetate (Zn), and dry acetonitrile were purchased from Sigma-Aldrich and used without further purification. Ethyl alcohol, 200 proof, was purchased from Fisher Scientific. 1,3,5,7-tetramethyl-2,6-diethyl-8-(4-carboxyphenyl)-4,4-difluoro-4-bora-3a,4a-diaza-s-indacene (BODIPY) was purchased from PorphyChem and used without further purification. MoS_2 triangles on SiO_2/Si were purchased from 2D semiconductors.

MoS_2 Growth and Sample Preparation

Continuous films of monolayer MoS_2 samples were grown on Si/SiO_2 by metal−organic chemical vapor deposition (MOCVD), detailed in Kang et al.[13] Monolayer MoS_2 films were cut into 0.5 cm × 0.5 cm squares and heated in an uncovered glass Petri dish in a 250 °C oven for 2 h before molecular loading. Heated films were immediately submerged in 0.75 mL of 50 mM MBA for 48 h. Following loading, they were soaked in 200 proof ethanol for 24 h and then blown dry with N_2. To add the linking ion, MoS_2-MBA films were then immersed in 0.75 mL of 1 mM $Zn(OAc)_2$ in ethanol for 2 h. Films were then left to soak in 200 proof ethanol for 24 h and blown dry with N_2. To load BODIPY on MoS_2-MBA-Zn films, vials were fitted with a nitrogen balloon and a solution of 2.5 mM BODIPY in dry acetonitrile was added and left to load for 1 h. Samples were then soaked in 200 proof ethanol for 24 h and blown dry with N_2. All control samples were prepared using the same loading conditions for each molecular component.

Atomic Force Microscopy

AFM images were captured using a Bruker Multimode 8 AFM using AC Tapping mode at 1 Hz over a 10 μm × 10 μm area.

Raman Spectroscopy

Raman spectra were collected using a LabRAM HR Evolution Raman Microscope with 532 nm excitation (ND 5%) under 100× magnification using a 600 groove/mm grating, collecting and averaging 40 acquisitions. A high order polynomial background (10−13) was removed from data using the LabSpec6 software. Data presented is normalized to the MoS_2 A_{1g} peak.

X-ray Photoelectron Spectroscopy

XPS analysis was performed on a Kratos Axis Nova spectrometer using a monochromatic Al Kα source (1486.6 eV). The sample analysis area is 0.3 × 0.7 mm^2. High-resolution spectra were collected with 20 eV pass energy and a step size of 0.1 eV. Charge neutralization was performed using a coaxial low energy electron flood source. Calibration was done by setting the C 1s peak of adventitious carbon to 284.8 eV. Deconvolution of the high-resolution XPS spectra was performed in CasaXPS software using Lorentzian (Mo 3d, S 2s, C 1s) and asymmetric Lorentzian−Gaussian (70−30) (S 2p, Zn 2p) curves and a Shirley background.

Photoluminescence

Solution photoluminescence of BODIPY was collected using a Horiba Duetta-Bio fitted with a 75 W xenon arc lamp source (λ_{ex} = 550 nm) and CCD fluorescence detector. Full spectra film emission was measured using the above-described Raman Microscope. Full image film photoluminescence was measured using a using a Leica GSD/TIRFM Ground State Depletion Superresolution Microscope in epifluorescence mode with 527−537 nm excitation and an internal dichroic at 541 nm. An iXon Ultra EMCCD camera was used for high frame rate, low light imaging with low read noise and a 160x/1.43 oil 0.07 mm WD objective was used. Note, differences in excitation wavelength were used based on detector limitations in measuring high quantum yield emitters. BODIPY used in these studies is a well-studied, commercial dye that obeys Kasha's rule; as such, regardless of excitation wavelength, emission will only occur in appreciable yield from the lowest vibrational state in the excited state. Thus, these differences in excitation lines will not affect our conclusions drawn from photoluminescence experiments.

UV−Visible Absorption

A dual beam Shimadzu UV-3600 Plus UV−vis−NIR spectrophotometer with a double monochromator and 0.1 nm wavelength resolution was used to collect solution UV−visible absorption spectra.

■ RESULTS AND DISCUSSION

First Layer

Continuous MoS_2 was prepared via MOCVD with average domain sizes ranging from approximately 3−10 μm.[13] The high temperatures required for CVD growth generate chalcogen vacancies due to the volatility of chalcogenides; these defects serve as ideal candidates for covalent adsorption sites for thiolated molecules.[43,44] Before loading molecules, MoS_2 samples were heated for 2 h at 250 °C in order to remove surface adsorbates. X-ray Photoelectron Spectroscopy (XPS) was used to measure the C 1s region of heated and unheated samples, Figure 2.[45] Calibrating by setting a C 1s peak of adventitious carbon to 284.8 eV, we observed a change in the chemical species of carbon adsorbates on unheated versus heated substrates, Figure 2a,b. The Mo 3d region remains consistent before and after heating, with only minor changes suggestive of the loss of MoO_3 with heating, Figure S6.

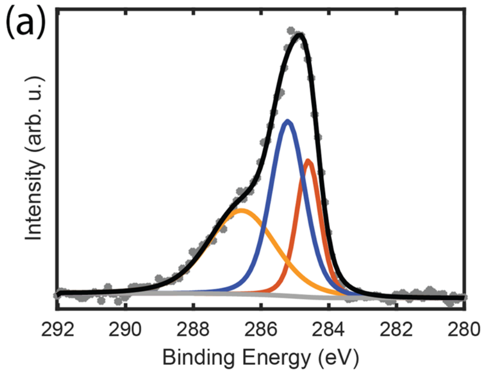

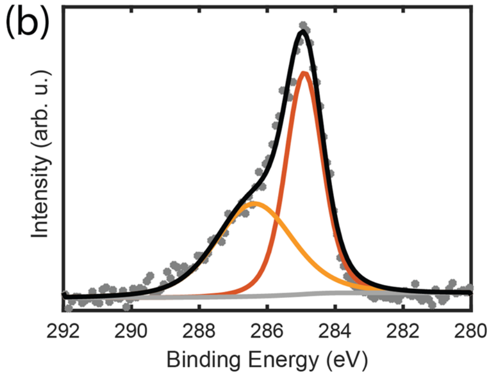

Figure 2. XPS spectra of the C 1s region of (a) unheated monolayer MoS_2 and (b) heated monolayer MoS_2.

We determined first layer adsorption of MBA onto monolayer MoS_2 using a combination of AFM and Raman spectroscopy. After loading MBA, samples were soaked in neat ethanol to remove any physisorbed molecules. There is debate surrounding the anchoring mechanism of first layer molecules. Reports propose molecular loading in the first step via S−H bond breaking in thiolated molecules and subsequent sulfur vacancy coordination by the deprotonated molecule[17,28,30,46] or physisorption of disulfides generated via thiol oxidation.[47] Using the motif proposed by Makarova et al., as thiol binding groups on MBA satisfy S-vacancies present in monolayer MoS_2, we expect the surface roughness of MoS_2 to increase, as the planar films will now be decorated with sporadic molecular attachments approximately 0.5 nm in size. Indeed, upon chemisorption, there is a notable increase in RMS surface roughness from 470 ± 14 to 730 ± 80 pm consistent with molecular attachment on MoS_2 after the washing process, Figure S1.[30] Note that we observe a large increase in roughness with soaking in neat ethanol (900 ± 100 pm), consistent with Raman changes, suggestive of potential ethanol loading and/or physisorption.[16] Oxygen is isoelectronic with sulfur, making it possible for oxygen passivation of some sulfur defects.[48] However, -SH groups out-compete ethanol coordination, making it possible for the adsorption of thiolated molecules to monolayer MoS_2, hence the difference in roughness upon MBA coordination.[18]

To further characterize MBA loading, we used Raman spectroscopy to monitor S-vacancy signatures in MoS_2, Figure 3. Monolayer MoS_2 has two characteristic Raman modes, E^1_{2g} (382 cm^{-1}) and A_{1g} (402.5 cm^{-1}), with a peak separation of 20.5 cm^{-1}, diagnostic of monolayer thickness.[49,50] Upon gentle heating, we observe no peak shifting or peak intensity effects, Figure S3. Upon adsorbing MBA to heated MoS_2, there is a high frequency shift of 3 cm^{-1} in the E^1_{2g} peak and a 2 cm^{-1} high frequency shift in the A_{1g} peak.

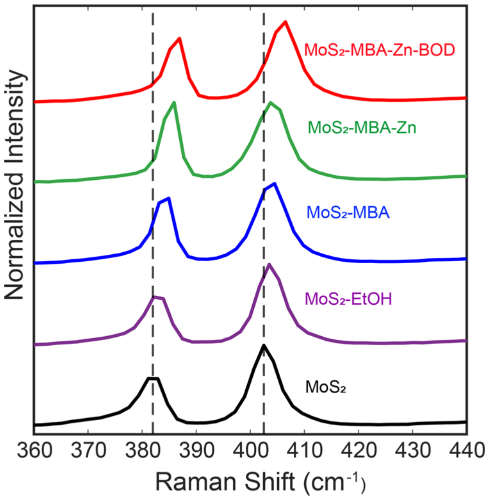

Figure 3. Raman spectra of monolayer MoS_2 (black), monolayer MoS_2 soaked in ethanol (purple), MoS_2-MBA (blue), MoS_2-MBA-Zn (green), and MoS_2-MBA-Zn-BODIPY (red).

The active E^1_{2g} mode describes the opposite, in plane vibration of Mo and S atoms in the lattice. In a vacancy-laden lattice, there are fewer Mo−S vibrations, reducing the restoring force,[51] and decreasing the frequency of the vibration.[52] As vacancies are filled upon the addition of MBA, we see a high frequency shift in these vibrations. The A_{1g} mode corresponds to out-of-plane S vibrations with a Mo center. In the presence of sulfur vacancies, there are fewer Mo−S vibrations (as in the case of the E^1_{2g} mode); however, static Mo centers become vibrationally active in the absence of a bonded sulfur, increasing the restoring force and increasing the frequency of the vibration. Thus, the restoring force increases with the addition of MBA as vacancies are satisfied, but more subtly, as seen by the more conservative shifting in the A_{1g} peak. Another signature of MBA adsorption is the increase in the E^1_{2g}:A_{1g} intensity ratio, Table S1.[35,53] Given the size of molecules used in this study, it may be possible for the small organics to migrate in between the MoS_2−substrate interface and induce molecular anchoring on the oxide surface. As previously reported, the E^1_{2g} and A_{1g} phonon modes are extremely sensitive to strain.[54,55] As such, one would expect that if there were a substrate−MoS_2 interruption caused by molecular loading and soaking, these effects would certainly manifest in the case of ethanol soaking; however, we note a remarkably similar Raman spectrum in this region before and after ethanol soaking.

In the absence of MBA, we do not observe Raman trends indicative of molecular loading, Figure S4. We also confirm that the mild heating conditions used for adsorbate removal does not affect Raman signatures, indicating the heating procedure does not induce any new sulfur vacancies, Figure S3.[45]

In order to ensure full loading, we conducted a concentration dependent loading study and found that the $I(E^1_{2g}):I(A_{1g})$ is unaffected by 5 mM MBA solution, but quickly approaches a near 1:1 ratio with concentrations ranging from 10 to 50 mM, Figure S5, Table S2. As such, subsequent studies use 50 mM loading solutions to achieve maximal loading of MBA to the available sulfur vacancies. Lastly, we were unable to observe vibrational signatures of MBA, $Zn(OAc)_2$, or BODIPY, Figure S2. This is likely due to low molecular concentration and thus low scatter intensity. Interestingly, we observe that upon bilayer growth, there are additional shifts in the MoS_2 phonon modes, Figure 3. It is unlikely that this is due to resolution of sulfur vacancies, per the full loading studies previously mentioned, and as such is suggestive of either a strain effect or modification of the dielectric environment manifesting in spectral changes. To investigate the loading of the linking ion and second layer, we explored a suite of spectroscopic techniques.

Ion Linkage

Following the covalent addition of MBA on heated MoS_2, samples were loaded in $Zn(OAc)_2$ in ethanol and left to soak in ethanol for 24 h to remove any noncoordinated Zn^{2+}. X-ray Photoelectron Spectroscopy (XPS) was then used to confirm the presence of a Zn^{2+} linking ion, Figure 4.

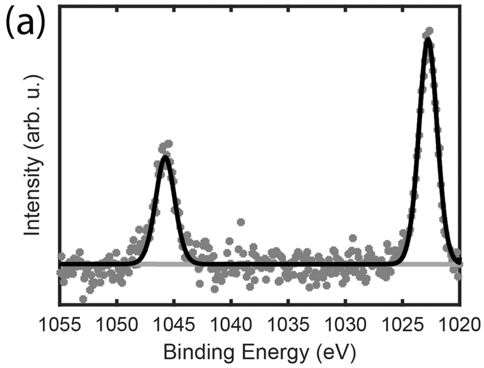

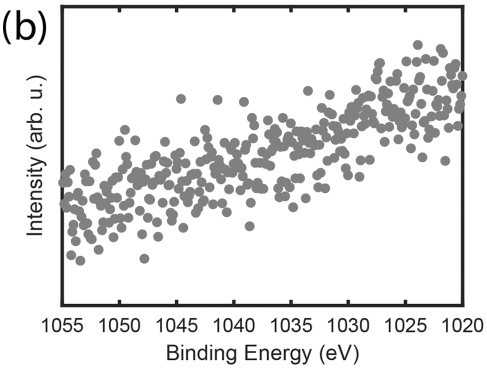

Figure 4. XPS spectra of the Zn 2p region of (a) MoS_2-MBA-Zn and (b) MoS_2-Zn.

We monitored the Zn 2p region using XPS to determine the loading of $Zn(OAc)_2$ and the required surface specificity of molecular binding groups. We observed no major influence of the ethanol soaking procedure on XPS results, Figure S10. Upon the adsorption of MBA, the unbound −COOH group acts as a coordination site for the addition of $Zn(OAc)_2$.[56] Note, the tetrahedral binding geometry of Zn(II) depicted in Figure 1 is an active area of research; the ion linkage is currently not well understood and there are ongoing efforts to describe the coordination geometry around the metal center. Zn carboxylate can be found as other typical dinuclear $[M_2(carboxylate)_4L_2]$ complexes displaying a paddle wheel like arrangement with solvent occupying axial coordination spots, and so each Zn(II) cation would be in a square-pyramidal coordination geometry.[57] Zn carboxylate can also be found as monomeric structures with two carboxylates and 2 solvent molecules, and thus have a pseudo-octahedral coordination environment. Both coordination geometries are possible and cannot be excluded.[58]

Zn 2p peaks appear in the XPS spectrum in the MoS_2-MBA-Zn sample with the Zn $2p_{1/2}$ and Zn $2p_{3/2}$ centered at 1045.63 and 1022.43 eV, respectively, with an energetic separation of 23.2 eV. This splitting is on the order of that observed in other Zn−O bonded environments, Figure 4a.[59] We observed that when we attempt to load $Zn(OAc)_2$ in the absence of covalently bound MBA, no Zn features are observed in the XPS spectrum, Figures 4b and S11. We are able to conclude from these studies that $Zn(OAc)_2$ cannot directly coordinate to sulfur vacancies in monolayer MoS_2, but instead loads via coordination to the −COOH groups on MBA. Furthermore, this also supports previous conclusions that there is binding group surface specificity as −SH groups are required for S-vacancy binding.[16,30] This ensures that surface nonspecific groups (like −COOH or $-PO_3H_2$) can be used for coordination to the linking ion without risk of competitive adsorption.

Due to the high concentration of sulfur in the intrinsic/pristine MoS_2 lattice, we were unable to determine the effects/concentrations of loaded thiols by monitoring the S 2p region as there are no observable changes in this regions upon loading, Figure S9. Additionally, there are no perceptible changes in the Mo 3d, S 2s, and C 1s regions, Figures S7 and S8. Finding a reliable way to quantify the number of sulfur vacancies before and after loading remains a priority and is a necessity for future studies to best understand these assemblies and their growth. There are current efforts in our lab focused on using desorptive methods to quantify first layer concentration.

Second Layer

MoS_2-MBA-Zn films were submerged in 2.5 mM BODIPY in dry acetonitrile and loaded under a nitrogen atmosphere for 1 h. Loading was followed by vigorous washing and a 24 h ethanol soak, after which samples were blown dry with N_2. Soaking with ethanol is necessary to remove physisorbed BODIPY. We observed that without soaking, XPS signatures of F are visible, Figure S12c. However, with the appropriate steps taken to avoid physisorption, this signature is too weak to be observed with the accessible resolution, Figure S12b. As XPS is sensitive to the present Zn(II) concentration, we would expect if BODIPY were at the same concentration, we would see observable F signatures upon coordination. As such, it is unlikely that we are forming an ILB for every Zn(II) site present, which is commonly observed for second layer loading due to steric restrictions on films.[60] This could possibly be ameliorated by using smaller second layer molecules, tailoring molecular orientation with judicious metal ion choice, or using targeted methods for vacancy generation to avoid molecular close packing.[16,61,62]

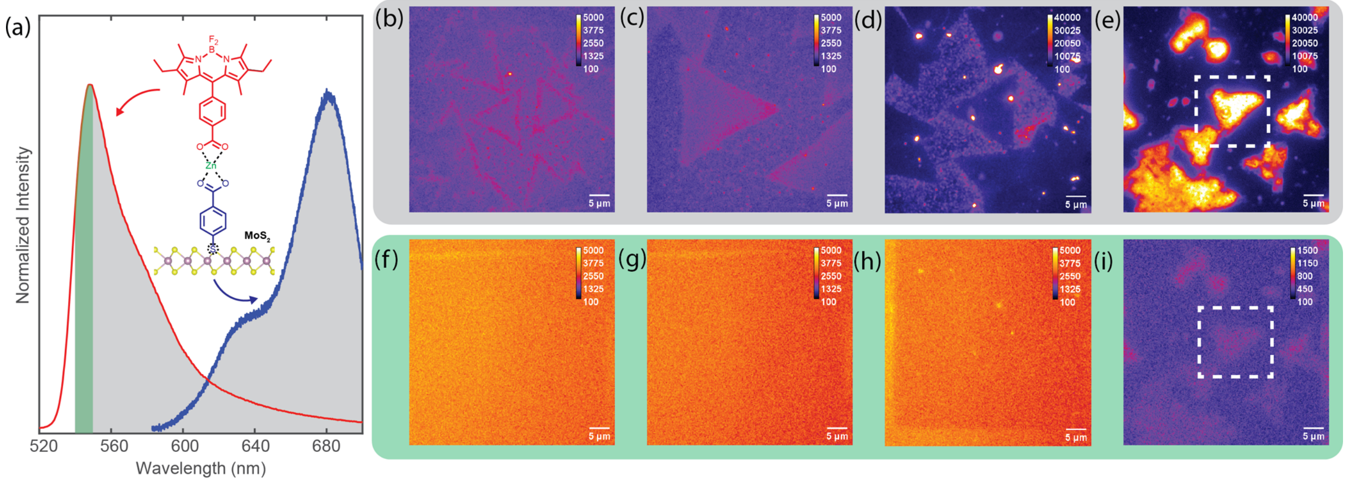

Figure 5. (a) Emission spectra of (red) BODIPY in acetonitrile (λ_{ex} = 550 nm) and (blue) nonfunctionalized monolayer MoS_2 (λ_{ex} = 532 nm). The green shaded region is indicative of the 540−550 nm region imaged in BODIPY selective PL microscopy experiments. PL microscopy images of MoS_2,MoS_2-MBA, MoS_2-MBA+BODIPY, and MoS_2-MBA-Zn-BODIPY (b−e) without (gray highlight) and (f−i) with a 550 nm short pass filter (green highlight).

Due to the insensitivity of XPS to the low coverage of BODIPY, PL microscopy was used to observe BODIPY emission and determine the presence of BODIPY in ion-linked bilayers on MoS_2, Figure 5. High sensitivity of emission measurements coupled with well-resolved peak separation in the emission spectra of monolayer MoS_2 and BODIPY, Figure 5a, makes PL microscopy an excellent technique to determine low concentration loading of BODIPY in the formed ILBs.[63] Note, in these measurements, we use CVD monolayer MoS_2 single crystal triangles that provide a geometric contrast against the Si/SiO_2 substrate. In PL microscopy, the samples are illuminated with 532 nm light that excites both BODIPY, Figure S14, and MoS_2 and emission is detected between (1) 540 and 700 nm, Figure 5b−e, and (2) 540 and 550 nm, Figure 5f−i. Condition (1) allows us to observe emission from both BODIPY and monolayer MoS_2, Figure 5a. Condition (2) utilizes a 550 nm short pass filter (FES550, Thorlabs), which only enables emission in the region highlighted in green in Figure 5a, excluding emission contribution from MoS_2 and allowing us to observe only BODIPY emission. Note, the short pass filter was used for its steep cut off that affords as narrow as possible detection for BODIPY emission, ensuring the goal of monitoring pure BODIPY emission for confirmation of second layer coordination. In bare MoS_2, Figure 5b,f, emission is observed most strongly at the edges of triangles. Others have cited high defect concentration at crystal edges as the cause of this behavior.[64] As S-vacancies are resolved with thiol containing MBA loading, there is a conservative decrease in edge site emission, Figure 5c. As expected, in both cases of bare MoS_2 and MoS_2-MBA, emissive contrast is lost when a 550 nm short pass filter is used and MoS_2 emission is filtered out, Figure 5f,g.

In MoS_2-MBA-Zn-BODIPY bilayers, we observe extremely strong emission in comparison to unmodified triangles, Figure 5e. When there is no ion linker present, strong emission is not localized to triangles, but rather appears in hot spots approximately 1 μm in size, Figure 5d. When a 550 nm short pass filter is placed in the line of detection to allow only for the detection of BODIPY emission, the substrate can only be distinguished from the flake geometry in the ILB sample, Figure 5h,i. Note, there are some bright spots present in MoS_2-MBA+BODIPY samples. Bright spots that appear localized on triangles are likely large deposits of physisorbed BODIPY not successfully removed by ethanol washing, while bright spots on the Si/SiO_2 substrate are a result of −COOH binding to the metal oxide surface, as these bright deposits are observable in the presence of the 550 nm short pass filter.[65−67]

These results suggest that in the presence of a Zn(II) ion linker, BODIPY is able to load via its axial −COOH group and generate an ILB. We do not observe BODIPY emission in samples where a BODIPY soak is completed in the absence of a linking ion, Figures 5h and S13c. There are two possible scenarios that could explain this, either (1) there is no physisorbtion or covalent adsorption of BODIPY to MoS_2 or (2) BODIPY is mildly physisorbed or adsorbed to MoS_2 via O-passivation of S-vacancies. In instance (2) we would expect to see no BODIPY emission, as the short distance between the two as well as the overlap between BODIPY emission (donor) and MoS_2 absorption (acceptor) would make for a FRET (Förster Resonance Energy Transfer) pair and quench the emission from adsorbed molecules.[63] As such, we cannot conclusively deduce if BODIPY can directly bind to MoS_2. Despite this limitation, we can conclude that the separation imposed by the ILB structure enables unquenched BODIPY emission in the second layer. This also provides general information regarding the orientation of the grown ILBs. We can be certain that the second layer orients near surface normal; in a lying down conformation, we would expect to see efficient FRET and minimal BODIPY emission.

CONCLUSIONS

Here, we report the growth and characterization of ion-linked bilayers consisting of a thiolated spacer, a Zn(II) linking ion, and a BODIPY fluorescent tag on monolayer MoS_2. First layer growth via S−H bond breaking and subsequent S-vacancy resolution was confirmed using AFM and Raman spectroscopy, where surface roughness and peak shifting were diagnostic of molecular loading, respectively. XPS analysis determined the coordination of Zn(II) in the presence of a carboxylate functionalized first layer molecule. Additionally, we further confirmed that acetate and carboxylate groups are not suitable surface binding groups for MoS_2. Lastly, PL microscopy confirmed the presence of second layer BODIPY only in the presence of a linking ion, and was suggestive of an average assembly orientation nearer to surface normal than a lying down conformation. Ultimately, we demonstrated the successful growth of an ion-linked bilayer on monolayer MoS_2.

ILBs hold the potential to introduce a host of new molecules onto sulfur containing TMDs without the need to develop new binding motifs. By simply layering desirable molecules with −COOH groups on top of spatially controlled −SH spacers, a new library of organic, inorganic, and even biomolecules are available. This simple growth strategy has the potential to inspire complex device designs that feature capabilities, like switchability, that are well controlled by molecular systems. The high tunability of structural components will allow researchers to methodically develop systems that can control multiple structural and electronic properties including second layer distance from surface, molecular orientation, and wave function overlap.

■ ASSOCIATED CONTENT

Supporting Information

The Supporting Information is available free of charge at https://pubs.acs.org/doi/10.1021/acsaom.4c00327.

> AFM, Raman spectroscopy, XPS, photoluminescence microscopy, and UV−visible absorption data for control samples (PDF)

■ AUTHOR INFORMATION

Corresponding Authors

Ashley Arcidiacono − *James Franck Institute, University of Chicago, Chicago, Illinois 60637, United States;* orcid.org/0000-0001-8617-2097; Email: aarcidiacono@uchicago.edu

Sarah B. King − *Department of Chemistry, University of Chicago, Chicago, Illinois 60637, United States; James Franck Institute, University of Chicago, Chicago, Illinois 60637, United States;* orcid.org/0000-0003-0274-9894; Email: sbking@uchicago.edu

Authors

Cooper R. Johnston − *Department of Chemistry, University of Chicago, Chicago, Illinois 60637, United States; James Franck Institute, University of Chicago, Chicago, Illinois 60637, United States*

Clare L. Keenan − *Department of Chemistry, University of Chicago, Chicago, Illinois 60637, United States; James Franck Institute, University of Chicago, Chicago, Illinois 60637, United States;* orcid.org/0000-0001-5652-2068

Nasim Mirzajani − *Department of Chemistry, University of Chicago, Chicago, Illinois 60637, United States; James Franck Institute, University of Chicago, Chicago, Illinois 60637, United States*

Anoushka Ghosh − *Department of Chemistry, University of Chicago, Chicago, Illinois 60637, United States*

Alexander S. Filatov − *Department of Chemistry, University of Chicago, Chicago, Illinois 60637, United States;* orcid.org/0000-0002-8378-1994

Complete contact information is available at: https://pubs.acs.org/10.1021/acsaom.4c00327

Notes

The authors declare no competing financial interest.

■ ACKNOWLEDGMENTS

This work was supported by the Office of Basic Energy Sciences, U.S. Department of Energy (Grant No. DE-SC0021950). A.A. acknowledges the Arnold O. Beckman Postdoctoral Fellowship Program (10.13039/100000997). We thank the University of Chicago Integrated Light Microscopy Core, especially Dr. Lorraine Horwitz and Dr. Christine Labno, for their assistance with photoluminescence microscopy. (RRID SCR019197) This work was conducted using shared facilities at the University of Chicago Materials Research Science and Engineering Center, supported by the National Science Foundation under award number DMR-2011854. Parts of this work were carried out at the Soft Matter Characterization Facility of the University of Chicago.

■ REFERENCES

(1) Yang, R.; Fan, Y.; Zhang, Y.; Mei, L.; Zhu, R.; Qin, J.; Hu, J.; Chen, Z.; Hau Ng, Y.; Voiry, D.; Li, S.; Lu, Q.; Wang, Q.; Yu, J. C.; Zeng, Z. 2D Transition Metal Dichalcogenides for Photocatalysis. *Angew. Chem., Int. Ed.* **2023**, *62*, e202218016.

(2) Peng, W.; Li, Y.; Zhang, F.; Zhang, G.; Fan, X. Roles of Two-Dimensional Transition Metal Dichalcogenides as Cocatalysts in Photocatalytic Hydrogen Evolution and Environmental Remediation. *Ind. Eng. Chem. Res.* **2017**, *56*, 4611−4626.

(3) Nassiri Nazif, K.; Nitta, F. U.; Daus, A.; Saraswat, K. C.; Pop, E. Efficiency limit of transition metal dichalcogenide solar cells. *Commun. Phys.* **2023**, *6*, 1−11.

(4) Nalwa, H. S. A review of molybdenum disulfide (MoS_2) based photodetectors: from ultra-broadband, self-powered to flexible devices. *RSC Adv.* **2020**, *10*, 30529−30602.

(5) Liu, Y.; Lin, L.; Sun, H.-B. Optical Modification of Two-Dimensional Materials: From Atomic to Electronic Scale. *J. Phys. Chem. C* **2024**, *128*, 2271−2290.

(6) Mueller, T.; Malic, E. Exciton physics and device application of two-dimensional transition metal dichalcogenide semiconductors. *2D Mater. Appl.* **2018**, *2*, 1−12.

(7) Wang, Y.; Slassi, A.; Stoeckel, M.-A.; Bertolazzi, S.; Cornil, J.; Beljonne, D.; Samorì, P. Doping of Monolayer Transition-Metal Dichalcogenides via Physisorption of Aromatic Solvent Molecules. *J. Phys. Chem. Lett.* **2019**, *10*, 540−547.

(8) Gao, H.; Suh, J.; Cao, M. C.; Joe, A. Y.; Mujid, F.; Lee, K.-H.; Xie, S.; Poddar, P.; Lee, J.-U.; Kang, K.; Kim, P.; Muller, D. A.; Park, J. Tuning Electrical Conductance of MoS $_2$ Monolayers through Substitutional Doping. *Nano Lett.* **2020**, *20*, 4095−4101.

(9) Younas, R.; Zhou, G.; Hinkle, C. L. A perspective on the doping of transition metal dichalcogenides for ultra-scaled transistors: Challenges and opportunities. *Appl. Phys. Lett.* **2023**, *122*, 160504.

(10) Devakul, T.; Crépel, V.; Zhang, Y.; Fu, L. Magic in twisted transition metal dichalcogenide bilayers. *Nat. Commun.* **2021**, *12*, No. 6730.

(11) Peng, Z.; Chen, X.; Fan, Y.; Srolovitz, D. J.; Lei, D. Strain engineering of 2D semiconductors and graphene: from strain fields to band-structure tuning and photonic applications. *Light Sci. Appl.* **2020**, *9*, 190.

(12) Zhou, X.; Hao, H.; Zhang, Y.-J.; Zheng, Q.; Tan, S.; Zhao, J.; Chen, H.-B.; Chen, J.-J.; Gu, Y.; Yu, H.-Q.; Liu, X.-W. Patterning of transition metal dichalcogenides catalyzed by surface plasmons with atomic precision. *Chem.* **2021**, *7*, 1626−1638.

(13) Kang, K.; Xie, S.; Huang, L.; Han, Y.; Huang, P. Y.; Mak, K. F.; Kim, C.-J.; Muller, D.; Park, J. High-mobility three-atom-thick semiconducting films with wafer-scale homogeneity. *Nature* **2015**, *520*, 656−660.

(14) Wang, X.; Feng, H.; Wu, Y.; Jiao, L. Controlled Synthesis of Highly Crystalline MoS_2 Flakes by Chemical Vapor Deposition. *J. Am. Chem. Soc.* **2013**, *135*, 5304−5307.

(15) Wan, Y.; Li, E.; Yu, Z.; Huang, J.-K.; Li, M.-Y.; Chou, A.-S.; Lee, Y.-T.; Lee, C.-J.; Hsu, H.-C.; Zhan, Q.; Aljarb, A.; Fu, J.-H.; Chiu, S.-P.; Wang, X.; Lin, J.-J.; Chiu, Y.-P.; Chang, W.-H.; Wang, H.; Shi, Y.; Lin, N.; et al. Low-defect-density WS_2 by hydroxide vapor phase deposition. *Nat. Commun.* **2022**, *13*, No. 4149.

(16) Bertolazzi, S.; Bonacchi, S.; Nan, G.; Pershin, A.; Beljonne, D.; Samorì, P. Engineering Chemically Active Defects in Monolayer MoS_2 Transistors via Ion-Beam Irradiation and Their Healing via Vapor Deposition of Alkanethiols. *Adv. Mater.* **2017**, *29*, 1606760.

(17) Yu, Z.; Pan, Y.; Shen, Y.; Wang, Z.; Ong, Z.-Y.; Xu, T.; Xin, R.; Pan, L.; Wang, B.; Sun, L.; Wang, J.; Zhang, G.; Zhang, Y. W.; Shi, Y.; Wang, X. Towards intrinsic charge transport in monolayer molybdenum disulfide by defect and interface engineering. *Nat. Commun.* **2014**, *5*, No. 5290.

(18) Cho, K.; Min, M.; Kim, T.-Y.; Jeong, H.; Pak, J.; Kim, J.-K.; Jang, J.; Yun, S. J.; Lee, Y. H.; Hong, W.-K.; Lee, T. Electrical and Optical Characterization of MoS_2 with Sulfur Vacancy Passivation by Treatment with Alkanethiol Molecules. *ACS Nano* **2015**, *9*, 8044−8053.

(19) Presolski, S.; Pumera, M. Covalent functionalization of MoS_2. *Mater. Today* **2016**, *19*, 140−145.

(20) Obaidulla, S. M.; Habib, M. R.; Khan, Y.; Kong, Y.; Liang, T.; Xu, M. MoS_2 and Perylene Derivative Based Type-II Heterostructure: Bandgap Engineering and Giant Photoluminescence Enhancement. *Adv. Mater. Interfaces* **2020**, *7*, 1901197.

(21) Amsterdam, S. H.; Stanev, T. K.; Zhou, Q.; Lou, A. J.-T.; Bergeron, H.; Darancet, P.; Hersam, M. C.; Stern, N. P.; Marks, T. J. Electronic Coupling in Metallophthalocyanine−Transition Metal Dichalcogenide Mixed-Dimensional Heterojunctions. *ACS Nano* **2019**, *13*, 4183−4190.

(22) Brkić, A. L.; Supina, A.; Ćapeta, D.; Dončević, L.; Ptiček, L.; Mandić, S.; Racan, L.; Delaš, I. Influence of Solvents and Adsorption of Organic Molecules on the Properties of CVD Synthesized 2D MoS_2. *Nanomaterials* **2023**, *13*, 2115.

(23) Saha, D.; Angizi, S.; Darestani-Farahani, M.; Dalmieda, J.; Selvaganapathy, P. R.; Kruse, P. Tuning the Chemical and Mechanical Properties of Conductive MoS_2 Thin Films by Surface Modification with Aryl Diazonium Salts. *Langmuir* **2022**, *38*, 3666−3675.

(24) Park, Y.; Shin, S.; An, Y.; Ahn, J.-G.; Shin, G.; Ahn, C.; Bang, J.; Baik, J.; Kim, Y.; Jung, J.; Lim, H. Tunable Optical Transition in 2H-MoS_2 via Direct Electrochemical Engineering of Vacancy Defects and Surface S−C Bonds. *ACS Appl. Mater. Interfaces* **2020**, *12*, 40870−40878.

(25) Im, H.; Bala, A.; So, B.; Kim, Y. J.; Kim, S. Customization of MoS_2 Phototransistors via Thiol-Based Functionalization. *Adv. Electron. Mater.* **2021**, *7*, 2100644.

(26) Tuci, G.; Mosconi, D.; Rossin, A.; Luconi, L.; Agnoli, S.; Righetto, M.; Pham-Huu, C.; Ba, H.; Cicchi, S.; Granozzi, G.; Giambastiani, G. Surface Engineering of Chemically Exfoliated MoS_2 in a "Click": How To Generate Versatile Multifunctional Transition Metal Dichalcogenides-Based Platforms. *Chem. Mater.* **2018**, *30*, 8257−8269.

(27) Vera-Hidalgo, M.; Giovanelli, E.; Navío, C.; Pérez, E. M. Mild Covalent Functionalization of Transition Metal Dichalcogenides with Maleimides: A "Click" Reaction for 2H-MoS_2 and WS_2. *J. Am. Chem. Soc.* **2019**, *141*, 3767−3771.

(28) Makarova, M.; Okawa, Y.; Aono, M. Selective Adsorption of Thiol Molecules at Sulfur Vacancies on MoS_2(0001), Followed by Vacancy Repair via S−C Dissociation. *J. Phys. Chem. C* **2012**, *116*, 22411−22416.

(29) Moehl, T.; Halim, M. A. E.; Tributsch, H. Photoelectrochemical studies on the n-MoS_2−Cysteine interaction. *J. Appl. Electrochem.* **2006**, *36*, 1341−1346.

(30) Sim, D. M.; Kim, M.; Yim, S.; Choi, M.-J.; Choi, J.; Yoo, S.; Jung, Y. S. Controlled Doping of Vacancy-Containing Few-Layer MoS_2 via Highly Stable Thiol-Based Molecular Chemisorption. *ACS Nano* **2015**, *9*, 12115−12123.

(31) Ding, Q.; Czech, K. J.; Zhao, Y.; Zhai, J.; Hamers, R. J.; Wright, J. C.; Jin, S. Basal-Plane Ligand Functionalization on Semiconducting 2H-MoS_2 Monolayers. *ACS Appl. Mater. Interfaces* **2017**, *9*, 12734−12742.

(32) Chu, X. S.; Yousaf, A.; Li, D. O.; Tang, A. A.; Debnath, A.; Ma, D.; Green, A. A.; Santos, E. J. G.; Wang, Q. H. Direct Covalent Chemical Functionalization of Unmodified Two-Dimensional Molybdenum Disulfide. *Chem. Mater.* **2018**, *30*, 2112−2128.

(33) Arcidiacono, A.; Hanks, B.; Hanson, K. Metal Ion-Linked Molecular Multilayers on Inorganic Substrates: Structure and Applications. *ACS Appl. Opt. Mater.* **2023**, *1*, 1156−1168.

(34) Lee, H.; Kepley, L. J.; Hong, H. G.; Mallouk, T. E. Inorganic analogs of Langmuir-Blodgett films: adsorption of ordered zirconium 1,10-decanebisphosphonate multilayers on silicon surfaces. *J. Am. Chem. Soc.* **1988**, *110*, 618−620.

(35) Zhang, L.; Cole, J. M. Anchoring Groups for Dye-Sensitized Solar Cells. *ACS Appl. Mater. Interfaces* **2015**, *7*, 3427−3455.

(36) Kaliginedi, V.; Ozawa, H.; Kuzume, A.; Maharajan, S.; Pobelov, I. V.; Kwon, N. H.; Mohos, M.; Broekmann, P.; Fromm, K. M.; Haga, M.-a.; Wandlowski, T. Layer-by-layer grown scalable redox-active ruthenium-based molecular multilayer thin films for electrochemical applications and beyond. *Nanoscale* **2015**, *7*, 17685−17692.

(37) Shan, B.; Vanka, S.; Li, T.-T.; Troian-Gautier, L.; Brennaman, M. K.; Mi, Z.; Meyer, T. J. Binary molecular-semiconductor p−n junctions for photoelectrocatalytic CO2 reduction. *Nat. Energy* **2019**, *4*, 290−299.

(38) Shan, B.; Nayak, A.; Brennaman, M. K.; Liu, M.; Marquard, S. L.; Eberhart, M. S.; Meyer, T. J. Controlling Vertical and Lateral Electron Migration Using a Bifunctional Chromophore Assembly in Dye-Sensitized Photoelectrosynthesis Cells. *J. Am. Chem. Soc.* **2018**, *140*, 6493−6500.

(39) Farnum, B. H.; Wee, K.-R.; Meyer, T. J. Self-assembled molecular p/n junctions for applications in dye-sensitized solar energy conversion. *Nature Chem.* **2016**, *8*, 845−852.

(40) Kobayashi, A. Photoredox Cascade Catalyst for Efficient Hydrogen Production with Biomass Photoreforming. *Angew. Chem.* **2023**, *135*, e202313014.

(41) Abdelrazzaq, F. B.; Kwong, R. C.; Thompson, M. E. Photocurrent Generation in Multilayer Organic-Inorganic Thin Films with Cascade Energy Architectures. *J. Am. Chem. Soc.* **2002**, *124*, 4796−4803.

(42) Ogunsolu, O. O.; Murphy, I. A.; Wang, J. C.; Das, A.; Hanson, K. Energy and Electron Transfer Cascade in Self-Assembled Bilayer Dye-Sensitized Solar Cells. *ACS Appl. Mater. Interfaces* **2016**, *8*, 28633−28640.

(43) Zafar, A.; Nan, H.; Zafar, Z.; Wu, Z.; Jiang, J.; You, Y.; Ni, Z. Probing the intrinsic optical quality of CVD grown MoS_2. *Nano Res.* **2017**, *10*, 1608−1617.

(44) Tomar, R.; Hsu, B.; Perez, A.; Stroscio, M.; Dutta, M. Probing Sulfur Vacancies in CVD-Grown Monolayer MoS_2 on SiO2/Si in the Temperature Range 750−900°C. *J. Electron. Mater.* **2023**, *52*, 5513−5520.

(45) Mitterreiter, E.; Schuler, B.; Micevic, A.; Hernangómez-Pérez, D.; Barthelmi, K.; Cochrane, K. A.; Kiemle, J.; Sigger, F.; Klein, J.; Wong, E.; Barnard, E. S.; Watanabe, K.; Taniguchi, T.; Lorke, M.; Jahnke, F.; Finley, J. J.; Schwartzberg, A. M.; Qiu, D. Y.; Refaely-Abramson, S.; Holleitner, A. W.; et al. The role of chalcogen vacancies for atomic defect emission in MoS_2. *Nat. Commun.* **2021**, *12*, No. 3822.

(46) Zonnevylle, M. C.; Hoffmann, R.; Harris, S. Thiophene hydrodesulfurization on MoS_2; Theoretical aspects. *Surf. Sci.* **1988**, *199*, 320−360.

(47) Chen, X.; Berner, N. C.; Backes, C.; Duesberg, G. S.; McDonald, A. R. Functionalization of Two-Dimensional MoS2: On the Reaction Between MoS2 and Organic Thiols. *Angew. Chem.* **2016**, *128*, 5897−5902.

(48) Lu, J.; Carvalho, A.; Chan, X. K.; Liu, H.; Liu, B.; Tok, E. S.; Loh, K. P.; Castro Neto, A. H.; Sow, C. H. Atomic Healing of Defects in Transition Metal Dichalcogenides. *Nano Lett.* **2015**, *15*, 3524−3532.

(49) Chakraborty, B.; Bera, A.; Muthu, D. V. S.; Bhowmick, S.; Waghmare, U. V.; Sood, A. K. Symmetry-dependent phonon renormalization in monolayer MoS 2 transistor. *Phys. Rev. B* **2012**, *85*, 161403.

(50) Li, H.; Zhang, Q.; Yap, C. C. R.; Tay, B. K.; Edwin, T. H. T.; Olivier, A.; Baillargeat, D. From Bulk to Monolayer MoS_2: Evolution of Raman Scattering. *Adv. Funct. Mater.* **2012**, *22*, 1385−1390.

(51) Rai, N. K.; Lakshmanna, A. Y.; Namboodiri, V. V.; Umapathy, S. Basic principles of ultrafast Raman loss spectroscopy. *J. Chem. Sci.* **2012**, *124*, 177−186.

(52) Parkin, W. M.; Balan, A.; Liang, L.; Das, P. M.; Lamparski, M.; Naylor, C. H.; Rodríguez-Manzo, J. A.; Johnson, A. T. C.; Meunier, V.; Drndić, M. Raman Shifts in Electron-Irradiated Monolayer MoS_2. *ACS Nano* **2016**, *10*, 4134−4142.

(53) Mignuzzi, S.; Pollard, A. J.; Bonini, N.; Brennan, B.; Gilmore, I. S.; Pimenta, M. A.; Richards, D.; Roy, D. Effect of disorder on Raman scattering of single-layer Mo S 2. *Phys. Rev. B* **2015**, *91*, 195411.

(54) Velický, M.; Rodriguez, A.; Bouša, M.; Krayev, A. V.; Vondráček, M.; Honolka, J.; Ahmadi, M.; Donnelly, G. E.; Huang, F.; Abruña, H. D.; Novoselov, K. S.; Frank, O. Strain and Charge Doping Fingerprints of the Strong Interaction between Monolayer MoS2 and Gold. *J. Phys. Chem. Lett.* **2020**, *11*, 6112−6118.

(55) Conley, H. J.; Wang, B.; Ziegler, J. I.; Haglund, R. F. J.; Pantelides, S. T.; Bolotin, K. I. Bandgap Engineering of Strained Monolayer and Bilayer MoS2. *Nano Lett.* **2013**, *13*, 3626−3630.

(56) Evans, S. D.; Ulman, A.; Goppert-Berarducci, K. E.; Gerenser, L. J. Self-assembled multilayers of.omega.-mercaptoalkanoic acids: selective ionic interactions. *J. Am. Chem. Soc.* **1991**, *113*, 5866−5868.

(57) Zhou, Q.; Hambley, T. W.; Kennedy, B. J.; Lay, P. A.; Turner, P.; Warwick, B.; Biffin, J. R.; Regtop, H. L. Syntheses and Characterization of Anti-inflammatory Dinuclear and Mononuclear Zinc Indomethacin Complexes. Crystal Structures of [Zn2-(Indomethacin)4(L)2] (L = N,N-Dimethylacetamide, Pyridine, 1-Methyl-2-pyrrolidinone) and [Zn(Indomethacin)2(L1)2] (L1 = Ethanol, Methanol). *Inorg. Chem.* **2000**, *39*, 3742−3748.

(58) Sánchez-Férez, F.; Pou, R.; Bayés-García, L.; Font-Bardia, M.; Pons, J.; Ayllón, J. A. Benzoate substituents effects on the structure of Zn(II) complexes and 1D 4,4'-bipyridine derived coordination polymers. *Inorg. Chim. Acta* **2020**, *500*, 119218.

(59) Barr, T. L.; Yin, M.; Varma, S. Detailed x-ray photoelectron spectroscopy valence band and core level studies of select metals oxidations. *J. Vac. Sci. Technol. A* **1992**, *10*, 2383−2390.

(60) Arcidiacono, A.; Zhou, Y.; Zhang, W.; Ellison, J. O.; Ayad, S.; Knorr, E. S.; Peters, A. N.; Zheng, L.; Yang, W.; Saavedra, S. S.; Hanson, K. Examining the Influence of Bilayer Structure on Energy Transfer and Molecular Photon Upconversion in Metal Ion Linked Multilayers. *J. Phys. Chem. C* **2020**, *124*, 23597−23610.

(61) Tsai, C.; Li, H.; Park, S.; Park, J.; Han, H. S.; Nørskov, J. K.; Zheng, X.; Abild-Pedersen, F. Electrochemical generation of sulfur vacancies in the basal plane of MoS_2 for hydrogen evolution. *Nat. Commun.* **2017**, *8*, No. 15113.

(62) Fujisawa, K.; Carvalho, B. R.; Zhang, T.; Perea-López, N.; Lin, Z.; Carozo, V.; Ramos, S. L. L. M.; Kahn, E.; Bolotsky, A.; Liu, H.; Elías, A. L.; Terrones, M. Quantification and Healing of Defects in Atomically Thin Molybdenum Disulfide: Beyond the Controlled Creation of Atomic Defects. *ACS Nano* **2021**, *15*, 9658−9669.

(63) Zhang, M.; Lihter, M.; Chen, T.-H.; Macha, M.; Rayabharam, A.; Banjac, K.; Zhao, Y.; Wang, Z.; Zhang, J.; Comtet, J.; Aluru, N. R.; Lingenfelder, M.; Kis, A.; Radenovic, A. Super-resolved Optical Mapping of Reactive Sulfur-Vacancies in Two-Dimensional Transition Metal Dichalcogenides. *ACS Nano* **2021**, *15*, 7168−7178.

(64) van der Zande, A. M.; Huang, P. Y.; Chenet, D. A.; Berkelbach, T. C.; You, Y.; Lee, G.-H.; Heinz, T. F.; Reichman, D. R.; Muller, D. A.; Hone, J. C. Grains and grain boundaries in highly crystalline monolayer molybdenum disulphide. *Nat. Mater.* **2013**, *12*, 554−561.

(65) Liu, Z.; Jiang, Z.; Yan, M.; Wang, X. Recent Progress of BODIPY Dyes With Aggregation-Induced Emission. *Front Chem.* **2019**, *7*, 712.

(66) Laurans, M.; Trinh, K.; Dalla Francesca, K.; Izzet, G.; Alves, S.; Derat, E.; Humblot, V.; Pluchery, O.; Vuillaume, D.; Lenfant, S.; Volatron, F.; Proust, A. Covalent Grafting of Polyoxometalate Hybrids onto Flat Silicon/Silicon Oxide: Insights from POMs Layers on Oxides. *ACS Appl. Mater. Interfaces* **2020**, *12*, 48109−48123.

(67) Murata, H.; Baskett, M.; Nishide, H.; Lahti, P. M. Adsorption of a Carboxylic Acid-Functionalized Aminoxyl Radical onto SiO2. *Langmuir* **2014**, *30*, 4026−4032.